The Plant Journal (2006) **46**, 351–368 doi: 10.1111/j.1365-313X.2006.02692.x

Metabolomic approaches reveal that phosphatidic and phosphatidyl glycerol phospholipids are major discriminatory non-polar metabolites in responses by *Brachypodium distachyon* to challenge by *Magnaporthe grisea*

J. William Allwood[1], David I. Ellis[2], Jim K. Heald[1], Royston Goodacre[2] and Luis A. J. Mur[1,*]

[1]*Institute of Biological Sciences, University of Wales, Aberystwyth, Edward Llwyd Building Ceredigion, Wales SY23 3DA, UK, and*

[2]*School of Chemistry, University of Manchester, PO Box 88, Sackville Street, Manchester M60 1QD, UK*

[*]For correspondence (fax +44 (0) 1970 622350; e-mail lum@aber.ac.uk).
Received 19 July 2005; revised 23 September 2005; accepted 14 November 2005.

Summary

Metabolomic approaches were used to elucidate some key metabolite changes occurring during interactions of *Magnaporthe grisea*– the cause of rice blast disease – with an alternate host, *Brachypodium distachyon*. Fourier-transform infrared (FT-IR) spectroscopy provided a high-throughput metabolic fingerprint of *M. grisea* interacting with the *B. distachyon* accessions ABR1 (susceptible) and ABR5 (resistant). Principal component–discriminant function analysis (PC-DFA) allowed the differentiation between developing disease symptoms and host resistance. Alignment of projected 'test-set' on to 'training-set' data indicated that our experimental approach produced highly reproducible data. Examination of PC-DFA loading plots indicated that fatty acids were one chemical group that discriminated between responses by ABR1 and ABR5 to *M. grisea*. To identify these, non-polar extracts of *M. grisea*-challenged *B. distachyon* were directly infused into an electrospray ionization mass spectrometer (ESI-MS). PC-DFA indicated that *M. grisea*-challenged ABR1 and ABR5 were differentially clustered away from healthy material. Subtraction spectra and PC-DFA loadings plots revealed discriminatory analytes (*m/z*) between each interaction and seven metabolites were subsequently identified as phospholipids (PLs) by ESI-MS-MS. Phosphatidyl glycerol (PG) PLs were suppressed during both resistant and susceptible responses. By contrast, different phosphatidic acid PLs either increased or were reduced during resistance or during disease development. This suggests considerable and differential PL processing of membrane lipids during each interaction which may be associated with the elaboration/suppression of defence mechanisms or developing disease symptoms.

Keywords: metabolomics, *magnaporthe grisea*, *Brachypodium distachyon*, phospholipids.

Introduction

The development of post-genomic approaches to assess biological problems is leading to rethinking of the standard 'hypothetico-deductive reductionist' approach to science (Goodacre *et al.*, 2004; Kell and Oliver, 2004). Whereas, classically, a hypothesis was tested by experimentation and then interpreted and the original hypothesis modified, the ability to collect extremely large datasets from various 'omic approaches, from carefully designed experiments, is allowing the development of computer-aided inductive approaches (Goodacre, 2003, 2005). The explanatory power of such inductive science is increased by maximizing the amount of relevant data. This is limited by experimental design and platform technology (Bino *et al.*, 2004; Dunn and Ellis, 2005), as well as the need for robust multivariate statistical analyses (Goodacre *et al.*, 2004). Further, each of the 'omic approaches has different advantages and disadvantages in offering a description of cell/organ/organism activity. Transcriptomics, for example, may report expression levels as low as one mRNA transcript per cell (Redman *et al.*, 2004) but mRNA and protein levels may be poorly correlated (Gygi

et al., 1999). Proteomics is being used in most fields of biology, but significant technical challenges remain (reviewed by Mann and Jensen, 2003; van Wijk, 2001). Further, if considering the control of metabolism, allosteric or feedback regulation will not be revealed by proteomic techniques (Fiehn and Weckwerth, 2003).

Metabolomics represents perhaps the ultimate level of 'omic analysis and within plant sciences is often the target of reverse genetic approaches (Fiehn, 2001, 2002; Hall *et al.*, 2002). Metabolomics will reveal changes in metabolite flux that are linked to only minor changes within either transcriptome or proteome (Urbanczyk-Wochniak *et al.*, 2003). Also unlike transcriptomics, metabolomic analysis aims to allow high-throughput processing of samples with large numbers of replicates so that statistically satisfying descriptions of many phenomena may be produced (Fiehn, 2001; Goodacre *et al.*, 2004). Moreover, metabolomics does not require extensive genomic sequence data so that, for example, the effects of genetic manipulation in potato (*Solanum tuberosum*) (Roessner *et al.*, 2001) and infection of *Catharanthus roseus* (Choi *et al.*, 2004) could be assessed. Nevertheless, plant metabolomic analysis poses its own problems, particularly the accurate detection of the large number of diverse metabolites using any of the differing technologies available, whether mass spectroscopy (MS) or nuclear magnetic resonance (NMR) (Dunn and Ellis, 2005; van der Greef *et al.*, 2004). These technologies notwithstanding, metabolite detection and peak deconvolution are not trivial, and statistically analysis of the large datasets needs to be rigorous (Hall *et al.*, 2002). In their pioneering work, Fiehn *et al.* (2000) used gas chromatography–mass spectrometry (GS-MS) to quantify 326 distinct compounds to distinguish between wild type and mutant accessions of Arabidopsis. Using a combination of cluster analysis and machine learning, this group and their collaborators have analysed sucrose metabolism in potato tubers and distinguished between two Arabidopsis accessions (Roessner *et al.*, 2001; Taylor *et al.*, 2002). Metabolomic approaches have also revealed subtle and yet significant metabolite changes in transgenic potato lines that expressed sucrose synthase isoform II but that failed to exhibit a phenotype (Weckwerth *et al.*, 2004). Metabolomics has the power to generate novel hypotheses, as shown in a recent study by Kaplan *et al.* (2004), where a large number of metabolites were revealed to be common to both heat and chilling stress in Arabidopsis. It is also possible to correlate metabolites with transcriptional changes in Arabidopsis (Hirai *et al.*, 2004).

To date, few metabolomic studies have investigated the effects of two interacting organisms. Narasimhan *et al.* (2003) used a combination of reverse-phase HPLC and electrospray ionization mass spectroscopy to (ESI-MS) to profile the 'rhizosphere metabolome' of root leaches from wild type and mutant Arabidopsis. Recently, a profile for *C. roseus* leaves infected with the phytoplasmas has been described (Choi *et al.*, 2004). In this work, principal components analysis (PCA) of ^{1}H-NMR spectra from phytoplasma infections were associated with increases in phenylpropanoids and terpenoid indole alkaloids. Our study focuses on a metabolomic analysis of interactions of the ascomycete pathogen *Magnaporthe grisea* with an alternate host, *Brachypodium distachyon* (Routledge *et al.*, 2004). *Magnaporthe grisea* is the causal agent of rice blast, a devastating disease that results in significant annual losses on crop yield (Baker *et al.*, 1997) and whose success is derived from a highly effective infection strategy (reviewed by Talbot, 2003). Briefly, this involves the germination of the conidium that has alighted on the hydrophobic leaf surface which forms a balloon-like appressorium on the emerging germ tube tip. Appressorial formation involves the conversion of glycogen to glycerol, achieving concentrations of approximately 3 M (Thines *et al.*, 2000). Inward water movement is accompanied by melanization of the appressorial surface layers which acts to retain water to generate phenomenal turgor pressures (8 MPa) and to drive a penetration peg through the plant cell wall. Appressorial formation and host penetration have been extensively characterized using mutants, but the processes governing *in planta* invasive growth have been less well characterized (Talbot, 2003). Mutations in aminophospholipid translocase (*PDE*) and neutral trehalase (*NTH1*) genes affect *in planta* fungal proliferation (Balhadere and Talbot, 2001; Foster *et al.*, 2003) but their roles are currently obscure. Unlike other fungal pathogens, toxins have not been implicated in *M. grisea* pathogenesis (Ou, 1985).

The exhibition of plant resistance to *M. grisea* has been associated with the elicitation of programmed cell death – the hypersensitive response (HR) - which has been linked with the localized generation of reactive oxygen species (ROS; Kawasaki *et al.*, 1999; Ono *et al.*, 2001) and the synthesis of antimicrobial phytoalexins (Nelson *et al.*, 1994; Umemura *et al.*, 2003). Resistance has also been correlated with distinctive patterns of defence gene expression, regulated by key chemical cues; for example, the phospholipid (PL)-derived jasmonate family (Lee *et al.*, 2001; Schweizer *et al.*, 1997). With the advent of post-genomic technologies, *M. grisea*–host interactions have been the focus of transcriptomic analyses using EST sequencing, microarray and serial analysis of gene expression (SAGE)-based approaches, although these have yet to yield many new insights (Kim *et al.*, 2001; Matsumura *et al.*, 2003; Rauyaree *et al.*, 2001; Shim *et al.*, 2004).

We have recently demonstrated the utility of a metabolic 'fingerprint', where prominent changes in the metabolome are revealed without identifying individual metabolites to generate biologically relevant data (Goodacre *et al.*, 2003; Johnson *et al.*, 2003; Kaderbhai *et al.*, 2003). Fourier-transform infrared (FT-IR) spectroscopy identified variables

between control and salt-stressed tomato (*Lycopersicon esculentum*) using principal component–discriminant function analysis (PC-DFA; Johnson *et al.*, 2003). In other work, the initiation of flowering in Morning Glory (*Pharbitis nil*) was analysed using direct-injection ESI-MS, where metabolites were discriminated using PC-DFA, artificial neural networks and genetic programming (Goodacre *et al.*, 2003). In this study, we apply both metabolic fingerprinting (FT-IR) and metabolic profiling approaches (ESI-MS) to analyse single resistance gene-mediated resistance to *M. grisea* and disease symptom development in *B. distachyon* which were very similar to those occurring in rice (*Oryza sativa*) (Routledge *et al.*, 2004). Based on FT-IR and ESI-MS, we demonstrate that *B. distachyon* produces highly reproducible and descriptive datasets which show distinctive genotypic and response-specific profiles. Some of these key discriminatory metabolites were unequivocally identified using tandem MS to be PLs, which are likely to be important in either disease development or the HR. These studies illustrated the potential of chemometric analysis of high-dimensional metabolite data from highly heterogeneous samples to derive targets and hypotheses for further investigation.

Results

Metabolic fingerprinting of the B. distachyon*/*M. grisea *pathosystem*

At 3 days, following challenge with *M. grisea* strain Guy11, *B. distachyon* accessions ABR1 and ABR5 exhibit indistinguishable, barely visible lesions (Routledge *et al.*, 2004). However, epifluorescent alanine blue-stained lesions in ABR5 at day 3 exhibited considerable callose deposition – a host response to infection – which was associated with little detectable hyphal development (Figure 1a). By contrast, infection sites in ABR1 exhibited little sign of callose and cells were characteristically filled with hyphae (Figure 1b). At 3 days, hyphae broke out of the first infected cell (Figure 1c) and at day 5, unlike in ABR5 (data not shown), substantial hyphal penetration of surrounding tissue was observed in ABR1 (Figure 1d).

To assess the metabolic fingerprint of events occurring at days 3 and 5 following challenge of *B. distachyon* ABR1 and ABR5 with *M. grisea*, FT-IR was employed. Unsurprisingly, FT-IR spectra from *M. grisea*-challenged plant and pure fungal samples were highly distinctive; however, there was very little obvious spectral variation between pathogen-infected plants and controls (Figure 2a). Hence, chemometric analysis using cluster analysis was used to assess whether these spectra contained enough (bio)chemical information to allow differentiation between infected plants and controls.

The unsupervised PCA, which models natural variability within the data, could not separate the FT-IR absorbance spectra of pathogen-challenged and control material (data not shown); this was attributable to plant-to-plant variability and has been observed by others (e.g. Fiehn *et al.*, 2000). Therefore, PC-DFA, a supervised technique, was performed on the principal components (PCs), with *a priori* knowledge of the number of classes, in this case, six treatments plus the controls. The resultant DFA ordination plots for ABR1 and ABR5 are shown in Figure 2(b,c), respectively; for ease of viewing, an average of three biological replicates per treatment is shown. In both ABR1 and ABR5, spraying with gelatine alone had a small effect on the metabolic fingerprints; however, this could not be explained simply by the addition of gelatine (data not shown) and suggested a response by the plant. Notwithstanding this, both accessions infected with *M. grisea* produced more distinctive metabolic fingerprints, indicating a greater host response.

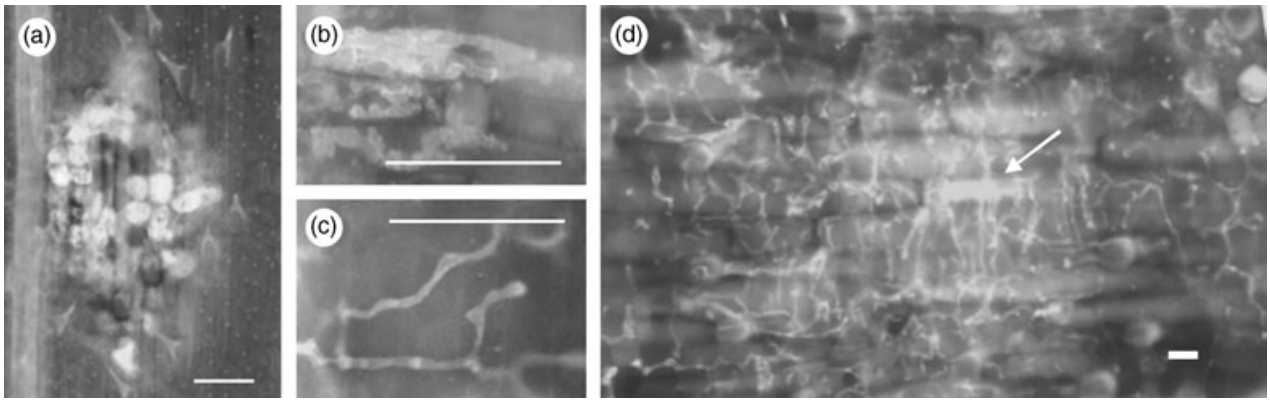

Figure 1. Epifluorescent alanine blue sites of *Magnaporthe grisea* Guy11 infection of *Brachypodium distachyon* accessions ABR1 and ABR5.
Alanine blue-stained infection sites of *M. grisea* strain Guy11 in *B. distachyon* accessions (a) ABR5 and (b) ABR1 at 3 days following challenge are shown viewed under UV illumination. Note the minimal fungal development in ABR5 with callose deposition in plant cells and the cell-filling hyphal development in ABR1. (c) In *B. distachyon* ABR1, fungal hyphal tips in cells adjacent to the original site of infection at 3 days following infection are shown. Note the bulbous tips. (d) Fungal spread in *B. distachyon* ABR1 at 5 days following challenge. The arrow indicates the originally infected cell. Bars, 100 μm.

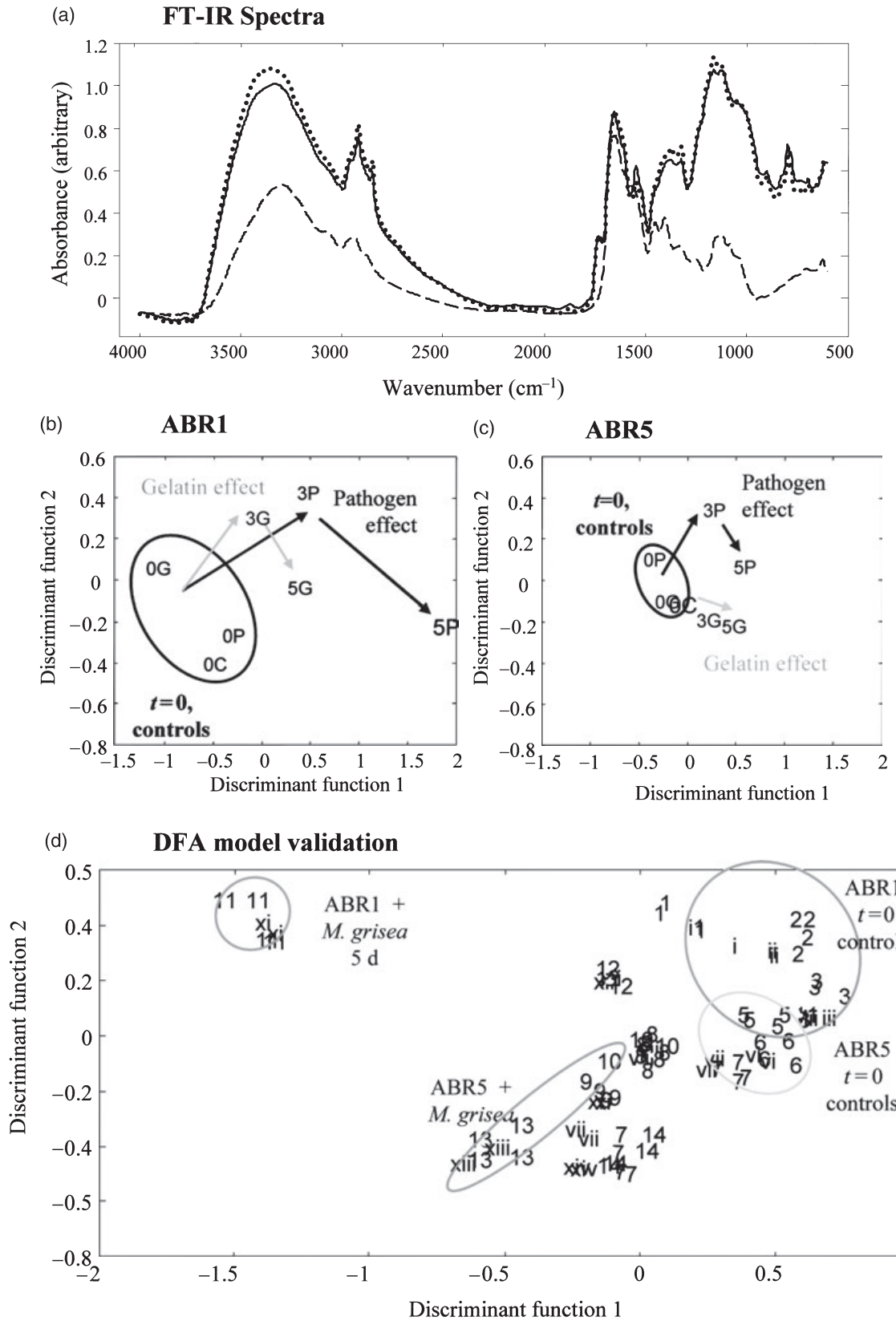

This response differed with time, and thus it was likely that FT-IR was detecting metabolite changes associated with the elaborating defence in ABR5, or lesion development in ABR1. Equilibrating and scaling the responses in DFA for either accession indicated that greater differences compared with controls were observed with the developing disease situation (Figure 2b compared to Figure 2c).

To validate each cluster and also differences between ABR1 and ABR5, both accessions were analysed together, and two biological replicates (so-called 'training' data) were used to construct PC-DFA and the third biological replicate was projected into this ordination space (Figure 2d). The projected 'test' data could be superimposed on top of their corresponding training data, which strongly suggested that highly reproducible experiment conditions had been attained. Given that these preliminary studies were based on a small number of biological replicates, these results indicated that our plant growth and infection procedures and analytical approach led to minimal sample-to-sample variation and thus our experimental approach was highly appropriate for more labour intensive and costly metabolic profiling. Figure 2 also clearly shows that the large metabolomic differences were to be seen in diseased samples after 5 days, as this group were recovered separately from all the other treatment groups in the first discriminant function which explains the majority of the total experimental variance.

We next sought to identify some of the metabolites giving rise to the variation seen with FT-IR. In order to study subtle difference in the host–parasite interaction, a 3-day timepoint was chosen as at this stage the *M. grisea* lesions are phenotypically indistinguishable, although some differential defence gene expression has been found (Routledge *et al.*, 2004). PC-DFA projection of FT-IR data (based on 10 PCs explaining 94.53% of the variance) from ABR1 and ABR5 challenged with *M. grisea* with gelatine and with gelatine alone revealed that DF1 readily discriminated between resistant (ABR5) and susceptible (ABR1) accessions, whilst DF2 described a common response to pathogenic challenge (Figure 3a). Individual PC-DFs are derived from DF loading vectors which are linear combinations of variables (here, IR wavenumbers) aiming to explain the observed variance (for further details, see Experimental procedures). The FT-IR spectrum is derived from the vibration of functional chemical groups and highly polar bonds so that particularly regions of the FT-IR spectrum are strongly influenced by particular molecule classes (Figure 3b). Thus, plotting loading vectors used for particular PC-DFs could indicate metabolites that contribute significantly to the variance. Loading plots for PC-DF1 (Figure 3c) and PC-DF2 (Figure 3d) indicated that metabolites within the amide and polysaccharide region contributed to differential and common ecotypic responses to pathogenic challenge. Additionally, a distinct group of fatty acid metabolites was observed (Figure 3c,d). In terms of identifying metabolites in complex mixtures, FT-IR does not have sufficient resolution and so we moved to a more targeted analysis. The fatty acid group was technically the easier to target using non-polar extraction procedures and this group also includes chemicals that are emerging as important defence signals (Meijer and Munnik, 2003); thus, our further analyses focused on non-polar metabolites.

Targeted metabolite profiling using direct injection ESI-MS

Non-polar extracts were profiled by direct infusion of extracts into ESI-MS operating in the negative ion mode (Goodacre *et al.*, 2002; Vaidyanathan *et al.*, 2002). To determine the optimum ESI sample cone voltage, samples were run at increasing cone voltages of 30, 40, 60, 80, and 100 V. Ion fragmentation was observed only at cone voltages of greater than 60 V. Although only non-polar extracts were analysed, information-rich spectra covering a wide range of metabolites from approximately 130 to 980 *m/z* were obtained (Figure S1). Data derived from each cone voltage were examined by PC-DFA. The best clustering in PC-DFA, as judged by the recovery of replicates after cluster reproducibility validation into tight groups, was found to be obtained using a cone voltage of 30 V (data not shown).

Figure 2. Fourier-transform infrared (FT-IR) spectra with discriminant function analysis (DFA) of *Magnaporthe grisea* Guy11 interactions with *Brachypodium distachyon* accessions ABR1 and ABR5.

(a) Example FT-IR spectra of extracts from *M. grisea* Guy11 alone (dashed line) and in *B. distachyon* accession ABR1 5 days following challenge with *M. grisea* Guy11 (dotted line) or spraying with 0.2% gelatine (solid line). DFA of FT-IR spectra of extracts of *B. distachyon* accessions (b) ABR1 and (c) ABR5 3 and 5 days following inoculation with *M. grisea* (0P, 3P and 5P indicate 0, 3 and 5 days following inoculation with pathogen) or 0.2% gelatine (0G, 3G and 5G indicate 0, 3 and 5 days following inoculation with gelatine), or for untreated controls (0C). Note that the number (0, 3 or 5) corresponds to the position of the data point. For (b) and (c), the points shown represent the mean DFA scores calculated from three biological and two machine replicates (i.e. six groups) for each treatment. The effects of pathogen inoculation or spraying with pathogen are indicated by arrows. Circles around day 0 samples are presented for clarity and have no mathematical significance. DFAs were based upon the first fifty PCs accounting for 95.822% of the total explained variance. (d) Validated DFA models for variance explained by application of *M. grisea* Guy11 and 0.2% gelatine mock infection in *B. distachyon* accessions ABR1 and ABR5 at 0, 3 and 5 days presented in (b) and (c). Validation involved deriving training datasets based on four replicates onto which the results of the two remaining replicates have been projected. This was based upon the first 25 PCs accounting for 97.31% of the total explained variance. Arabic numbers refer to training datasets and the corresponding roman numerals the test sets, as follows. (1, i) Uninoculated ABR1 controls; (2, ii) ABR1, day 0 after application of *M. grisea* in 0.2% gelatine; (3, iii) ABR1, day 0 with 0.2% gelatine; (4, iv) uninoculated ABR5 controls; (5, v) ABR5, day 0 after application of *M. grisea* in 0.2% gelatine; (6, vi) ABR5, day 0 with 0.2% gelatine; (7, vii) ABR1, day 3 after application of *M. grisea* in 0.2% gelatine; (8, viii) ABR1, day 3 with 0.2% gelatine; (9, ix) ABR5, day 3 after application of *M. grisea* in 0.2% gelatine; (10, x) ABR5, day 3 with 0.2% gelatine; (11, xi) ABR1, day 3 after application of *M. grisea* in 0.2% gelatine; (12 xii) ABR1, day 3 with 0.2% gelatine; (13, xiii) ABR5, day 3 after application of *M. grisea* in 0.2% gelatine, and (14, xiv) ABR5, day 3 with 0.2% gelatine. Circles around training and test sets are presented for clarity and have no mathematical significance.

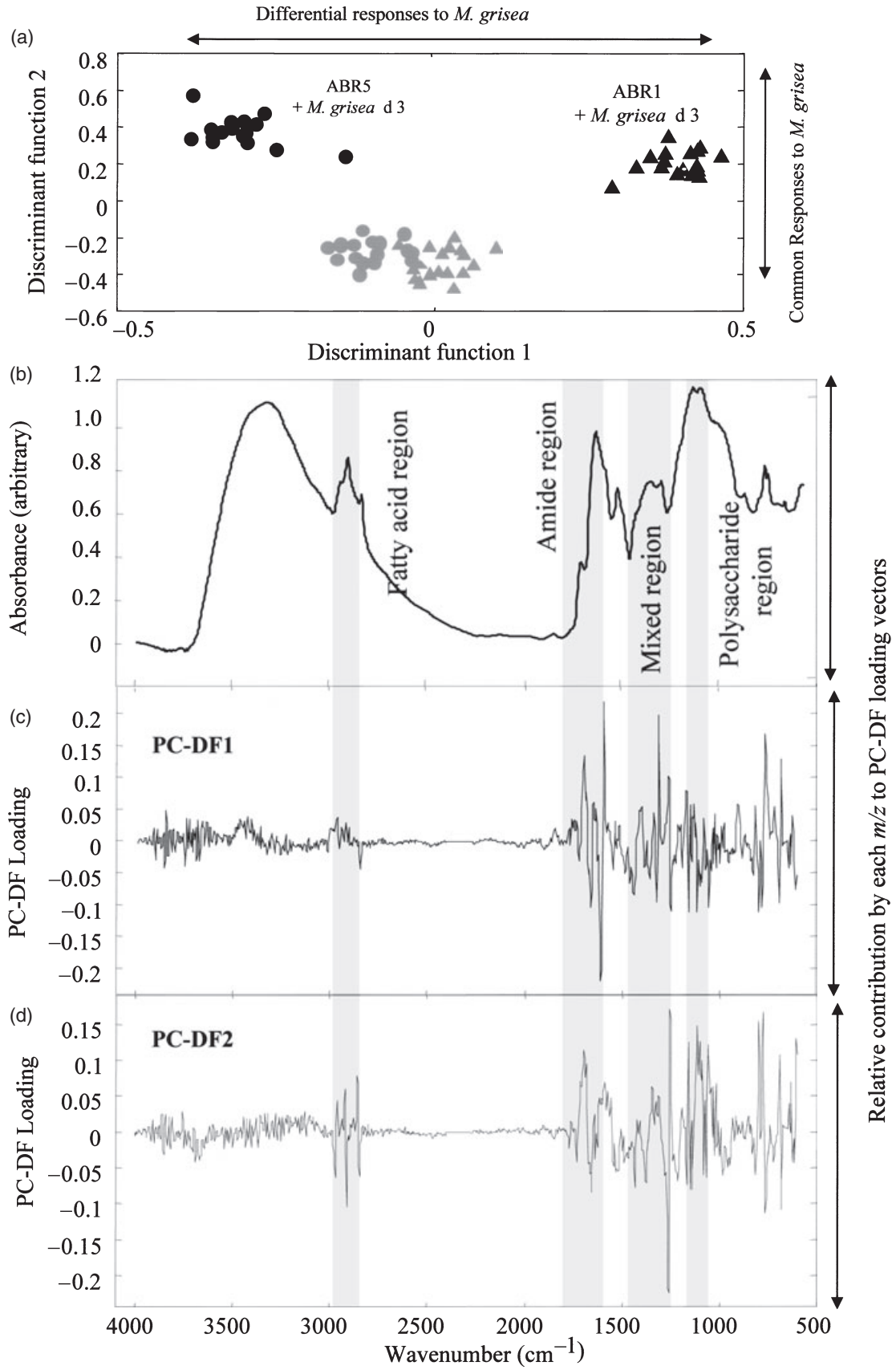

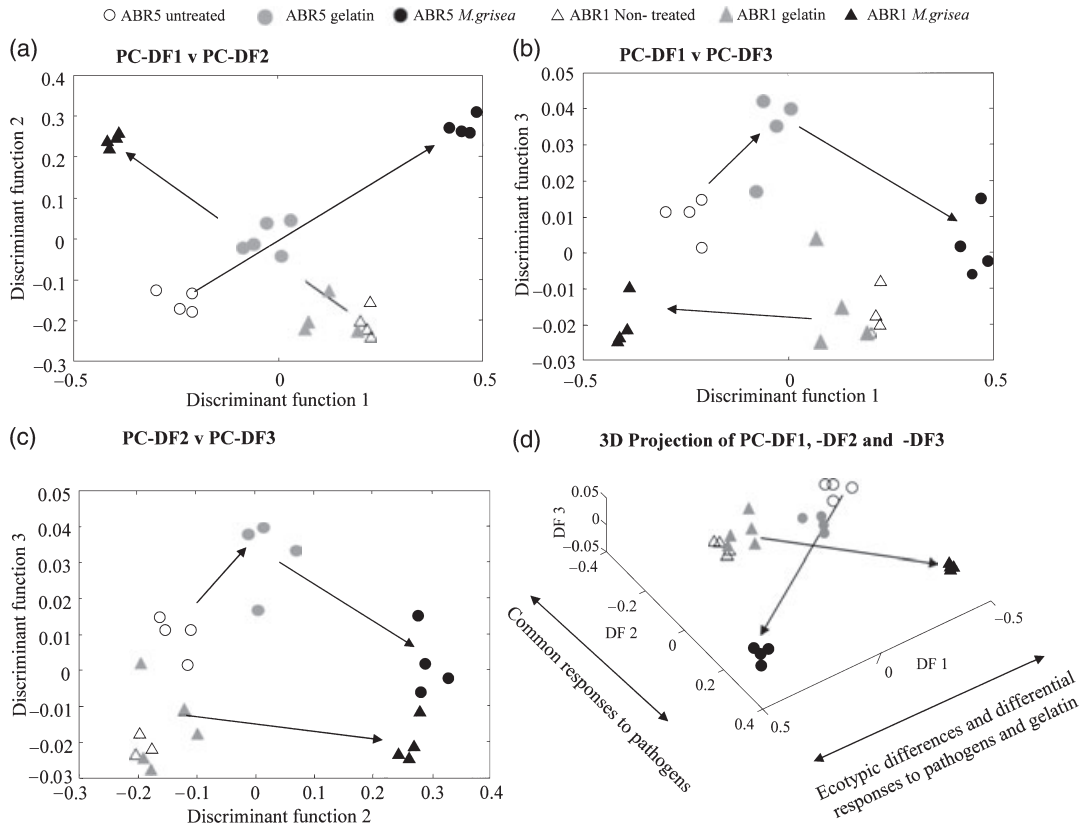

Figure 4. Discriminant function analysis (DFA) of electrospray ionization–mass spectrometry (ESI-MS) spectra of *Magnaporthe grisea* Guy11 interactions with *Brachypodium distachyon* accessions ABR1 and ABR5.
3D-DFA model of ESI-MS spectra of extracts from *B. distachyon* accessions ABR1 and ABR5 at 3 days following inoculation with *M. grisea* (ABR1, ▲; ABR5, ●) or spraying with 0.2% gelatine (ABR1, ▲; ABR5, ●), and from non-treated controls (ABR1, △; ABR5, ○). DFAs were based upon the first 10 PCs accounting for 99.27% of the total explained variance. The effects of pathogen inoculation or spraying with pathogen are indicated by arrows. DF1 explains variance attributable to application of *M. grisea* for both ABR1 lesion development and ABR5 resistance. DF2 explains variance attributable to common responses to *M. grisea* in the two accessions. DF3 explains basic ecotypic variation and some differential responses by ABR1 to gelatine spray.

PC-DFA was used to differentiate infected, non-challenged and gelatine-sprayed material from both accessions. All infected and control experimental groups showed tight clustering when four (results for this small number were used for ease of viewing) replicates were analysed by PC-DFA (Figure 4). PC-DFA based on the first 10 PCs (99.27% total explained variance) clearly discriminated between test and control sample groups. PC-DF1 explained much of the variance between responses of accessions ABR1 and ABR5 to *M. grisea* (Figure 4a,b), whereas PC-DF2 described common responses in the two accessions to fungal challenge (Figure 4a,c). PC-DF3 mostly explained basic ecotypic variation and some differential responses by ABR1 to gelatine spray (Figure 4b,c). A scaled 3D projection is included to aid visualization of the variation explained by each PC-DF (Figure 4d).

As previously performed in FT-IR (Figure 2d) to validate the cluster analysis, eight replicates were randomly chosen and used as a training set for PC-DFA, and two test replicates were projected into this ordinate space. The superimposition of training and test data into tight clusters again indicated a very high degree of agreement between data (not shown) and that the experimental approach used produced very reproducible data.

Identification of discriminatory metabolites by ESI-tandem MS and liquid chromatography–mass spectrometry (LC-MS)

Examination of DF loading vectors will identify ions used to derive the PC-DF models based on ten biological replicates. However, in our experiments, individual DF

Figure 3. Principal component–discriminant function analysis (PC-DFA) loading vectors (Eigenvalues) plotted against infrared (IR) wavenumbers.
(a) DFA model of Fourier-transform infrared (FT-IR) spectra of extracts from *Brachypodium distachyon* accessions ABR1 and ABR5 at 3 days following inoculation with *Magnaporthe grisea* (ABR1, ▲; ABR5, ●) or spraying with 0.2% gelatine (ABR1, ▲; ABR5, ●). DFAs were based upon the first 10 PCs accounting for 94.53% of the total explained variance. DF1 explains variance attributable to application of *M. grisea* for both ABR1 lesion development and ABR5 resistance. DF2 explains variance attributable to common responses to *M. grisea* in the two accessions. (b) An example FT-IR spectrum of an extract from *B. distachyon* accession ABR1 5 days following challenge with *M. grisea* Guy11. Indicated are parts of the spectrum where a metabolite group exhibits particular absorbance. PC-DFA loadings vectors are plotted against wavenumbers (cm^{-1}) for (c) PC-DF1 and (d) DC-DF2.

not only explained pathogen-induced but also (to variable extents) gelatine or ecotypic differences (Figure 4). Thus, discriminatory ions that contributed most to *M. grisea*-associated variance were identified in a two-stage process. Firstly, all replicates of pathogen-infected spectra for each accession and those corresponding to gelatine were averaged and subtraction spectra (*M. grisea*-challenged mean minus gelatine-treated mean) were derived for each accession. This approach targeted pathogen-elicited increases or decreases in metabolites at 3 days. The subtracted ions were then compared back to a plot of the DF loading vectors derived from non-averaged spectra to identify which *m/z* contributed most to variance. Figure 5(a) shows the loading vector *m/z* plots illustrating the *m/z* ion contribution to the variation in each PC-DF given in Figure 4.

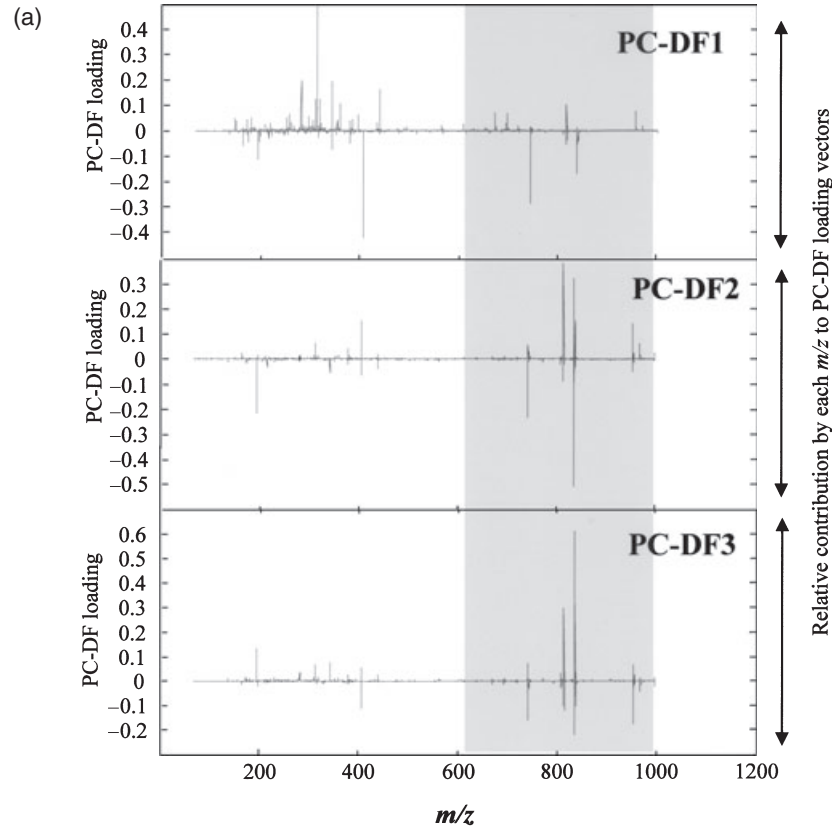

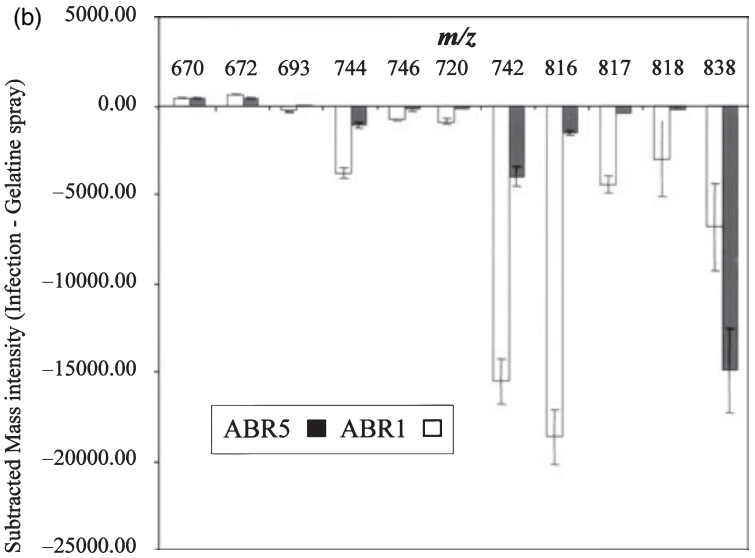

Figure 5. Principal component–discriminant function analysis (PC-DFA) loading vectors plotted against *m/z* and subtracted ion counts of discriminatory *m/z*.
(a) PC-DFA loadings vectors plotted against *m/z* revealing the major ions contributing variance in electrospray ionization–mass spectrometry (ESI-MS) spectra for *Brachypodium distachyon* accessions ABR1 and ABR5 and following application of either 0.2% gelatine or *Magnaporthe grisea* Guy11. DF1 accounted for 48.757%, DF2 accounted for 73.769% and DF3 accounted for 85.579% of the total explained variance. Loading plots were compared against a list of *m/z* derived from the subtraction of gelatine-treated mean spectra from *M. grisea*-treated mean spectra, for each of the accessions individually. (b) Ions that were prominent in both the subtraction spectra and the loading plots were considered key metabolites for identification.

None of the low-*m/z* ions that were prominent in the PC-DF1 loadings appeared in the subtraction spectra. This suggests that these low-*m/z* mass ions contributed to variance between the ABR1 and ABR5 accessions, or common responses to gelatine treatment (Figure 4d). For example, prominent *m/z* 131, 146, 195, and 313 were found to be several magnitudes greater in the normalized total ion count spectra for untreated ABR1 compared with ABR5, suggesting discrimination between the accessions. The *m/z* 191, 242, 341 377, 404 and 439 were found in equal magnitude in the two accessions; however, the addition of gelatine resulted in the down-regulation of all six *m/z* in both accessions and also *m/z* 131, 146, 195, and 313 in the ABR1 accession.

In examining *m/z* >600 (shaded in Figure 5a), it was noted that these discriminated common responses to pathogen challenge (i.e. in PC-DF2) and ecotypic variation (i.e. PC-DF3) as well as ecotypic-specific responses to *M. grisea* (i.e. PC-DF1). Referral to the subtraction spectra allowed ion changes specifically associated with pathogenic challenge to be targeted in each PC-DF. Using this approach, only 11 metabolites ranging between *m/z* 670 and 838 were highlighted as discriminatory between *M. grisea*-challenged and control plants (Table 1). The subtracted normalized ion counts (gelatine versus *M. grisea* + gelatine-treated) for each discriminatory *m/z* are given in Figure 5(b). This indicated the sensitivity of PC-DFA in detecting both large (e.g. *m/z* 816) and subtle (e.g. *m/z* 670) changes in metabolites. As an independent confirmation of significance, analyses of variance (ANOVAs) were undertaken of normalized ions counts from individual spectra for each of these ions, where the values from *M. grisea*-challenged samples were compared with those from both untreated and gelatine-treated controls (Table 1). ANOVAs suggested that six mass ions in the 720–746 *m/z* range as well as *m/z* 816 and 817 were significantly reduced ($P < 0.001$) whilst *m/z* 818 and 837 were significantly reduced only in ABR5. A greater variety of responses was observed with the other ions, *m/z* 670 being reduced in ABR5 and increased in ABR1 whilst the converse was observed with *m/z* 693. The ion counts of *m/z* 672 increased in both accessions following inoculation. ANOVA of ion counts from a selection of *m/z* that were not selected by PC-DFA did not reveal any significant differences.

Table 1 Discriminatory ions (*m/z*) during pathogenesis and the elicitation of resistance in the interaction of *Magnaporthe grisea* Guy11 and *Brachypodium distachyon* accessions ABR1 and ABR5

	Discriminatory function with *M. grisea*			
m/z	ABR1	ABR5	MS-MS daughter ions	Identification
670	+***	−***	409, 391, 277, 255, 153, 137	PA 16:0/18:3
672	+**	+***	409, 391, 279, 255, 153, 137	PA 16:0/18:2
693	−***	+**	433, 415, 279, 277, 153	PA 18:2/18:3
720	−***	−***	255, 253, 153	PG 16:0/16:1
742	−***	−***	505, 277, 253, 153	PG 16:1/18:3
744	−***	−***	507, 277, 255, 153	PG 16:0/18:3
746	−***	−***	465, 279, 255, 153	PG 16:0/18:2
816	−***	−***		Not identified
817	−***	−***		Not identified
818	NS (0.204)	−***		Not identified
838	NS (0.145)	−***		Not identified
648	Standard		409, 391, 255, 153	PA 16:0/16:0
748	Standard		465, 391, 281, 255, 153	PG 16:0/18:1

MS, mass spectrometry; PG, phosphatidyl glycerol; PA, phosphatidic acid. The fatty acid tails include palmitic acid (16:0), palmitoleic acid (16:1); linoleic acid (18:2); and linolenic acid (18:3).
***$P < 0.001$; **$P < 0.01$; NS, no significant increase (+) or decrease (−) in *M. grisea*-challenged samples compared with gelatine-treated and untreated controls of the same *B. distachyon* accession in analyses of variance.

Mass ions that discriminated between plant–pathogen interactions were tentatively identified as PLs by comparison with data from previous studies (Goodacre *et al.*, 2002) but we sought to confirm this by ESI-MS-MS. Of the 11 ions selected for MS-MS, seven possessed characteristics of PL spectra (Figure 6; Table 1) with the smallest daughter ions of 137 *m/z* (identified as a PL polar head) and 153 *m/z* (PL polar head bound to an oxygen atom). The next largest pair of masses was generated by R_2COO^- and R_1COO^- fragments (Table 2). The next four masses were generated by the polar head group of the PL having lost one of the following fragments: R_2COO^-, R_2CO^-, R_1COO^-, and R_1CO^- (given in order of increasing *m/z*). The largest fragment was generated by the intact PL, although an additional smaller mass may be generated by loss of the PL side-chain (R_3) (Brugger *et al.*, 1997; Fang and Barcelona, 1998; Goodacre *et al.*, 1999, 2002).

Mass ions that were reciprocally increased and decreased in each accession following challenge with *M. grisea* were phosphatidic acid (PA) PLs, PA with C16:0/18:3 acyl tails (670 *m/z*), PA C16:0/18:2 (672 *m/z*) and PA C18:2/18:3 (693 *m/z*) (Figure 7; Table 1). PLs that were reduced in both resistant and disease-forming interactions were phosphatidyl glycerol (PG) PLs, PG C16:0/16:1 (720 *m/z*) PG C16:1/18:3 (742 *m/z*), PG C16:0/18:3 (744 *m/z*) and PG C16:0/18:2 (746 *m/z*) (Figure 8; Table 1). The averaged ion counts of all three of the latter PG PLs were found to be two to three orders greater in ABR5 than in ABR1, indicating differences in PL composition between the two accessions. To confirm that the identified metabolites were PA and PG PLs, standards of 1, 2-dipalmitoyl-sn-glycero-3-phosphate sodium salt (Figure 7) and 1-palmitoyl-2-oleoyl-sn-glycero-3-phospho-rac-(1-glycerol) ammonium salt (Figure 8) were analysed by ESI-MS. These standards produced equivalent fragmentation patterns, thereby confirming the plant extracted PL identities.

ESI-MS-MS of *m/z* 816, 817, 818 and 836 produced daughter ions that were identified as glycerol, C18:3 and the 153 *m/z* PL polar head. However, these spectra also

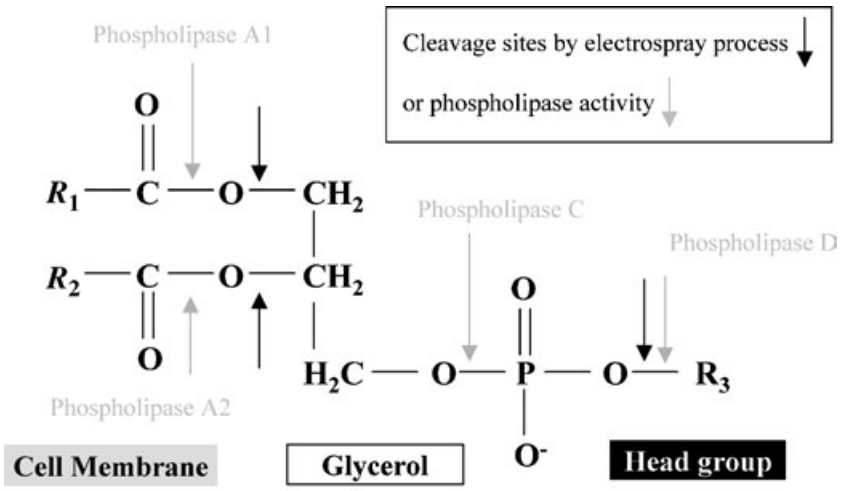

Figure 6. Phospholipid cleavage sites in the electrospray process and digestion with phospholipases.

Table 2 Calculated masses for the phospholipid R_1COO^- and R_2COO^- fatty acyl side-chain constituents, after their electrospray cleavage

Number of unsaturated bonds	Number of carbon atoms in fatty acyl chain					
	14	15	16	17	18	19
0	227	241	**255**	269	283	297
1	225	239	**253**	267	281	295
2	223	237	251	265	**279**	293
3	221	235	249	263	**277**	291

Masses in bold are the fatty acyl chains in the ESI-MS-MS of confirmed phospholipids.

contained a cluster of peaks of approximately 500 *m/z* which were not consistent with PL fragmentation and, unfortunately, this could not be resolved by LC-MS. No sugar moieties could be detected, indicating that these were not glycolipids. Based on their masses and our partial identification of their degradation products we suggest that these ions are likely to be derived from triglycerides.

It was noted that several discriminatory PLs had C18:3 acyl tails. As the oxylipin signal, jasmonic acid (JA), is derived from the linolenic acid (C18:3) fatty acids, we sought to correlate the reduction in PLs with the appearance of JA (Figure 9). Using targeted metabolite analysis, JA was observed to increase during both interactions at approximately 3 days but thereafter declined in ABR5, whilst in ABR1 levels were maintained.

Discussion

The application of metabolomic approaches to plants is still in its infancy. Plants exhibit an enormous chemical richness, encompassing as many as 200,000 metabolites (Pickersky and Gang, 2000), and this compounds problems associated with their detection and resolution (Fiehn, 2001). To date, most plant metabolomic studies have focused on comparing situations where there are large chemical differences, exhibited throughout the plant, for instance comparisons between mutant or transgenic and wild-type lines (e.g. Fiehn *et al.*, 2000; Roessner *et al.*, 2001) or heating and chilling stress (Kaplan *et al.*, 2004). By contrast, we applied metabolomic approaches to investigate localized interactions of a fungus and its host. This posed significant technical challenges as this interaction represented a dynamic situation where highly heterogeneous tissues (plant-infected cells, non-infected cells and fungal hyphae) were simultaneously sampled. This work therefore assessed the reproducibility of the metabolite changes and the robustness of multivariate statistical analysis to detect major relevant metabolite changes.

Use of a hierarchy of metabolomic approaches with multivariate statistics identifies metabolites that contribute to M. grisea–B. distachyon *interactions*

To begin to characterize the metabolome of this complex biological scenario, a fingerprinting technique was first used to establish the validity of the experimental conditions and design. Metabolic fingerprinting involves pattern recognition and a fast and relatively cheap 'first-round' screening approach which characterizes the (bio)chemical characteristics of a sample (Fiehn, 2001). Such an approach has proved to be enormously useful in scenarios such as bacterial identification (Vaidyanathan *et al.*, 2001), yeast mutant characterization (Raamsdonk *et al.*, 2001), drug toxicology trials and disease diagnosis (reviewed by Griffin, 2003).

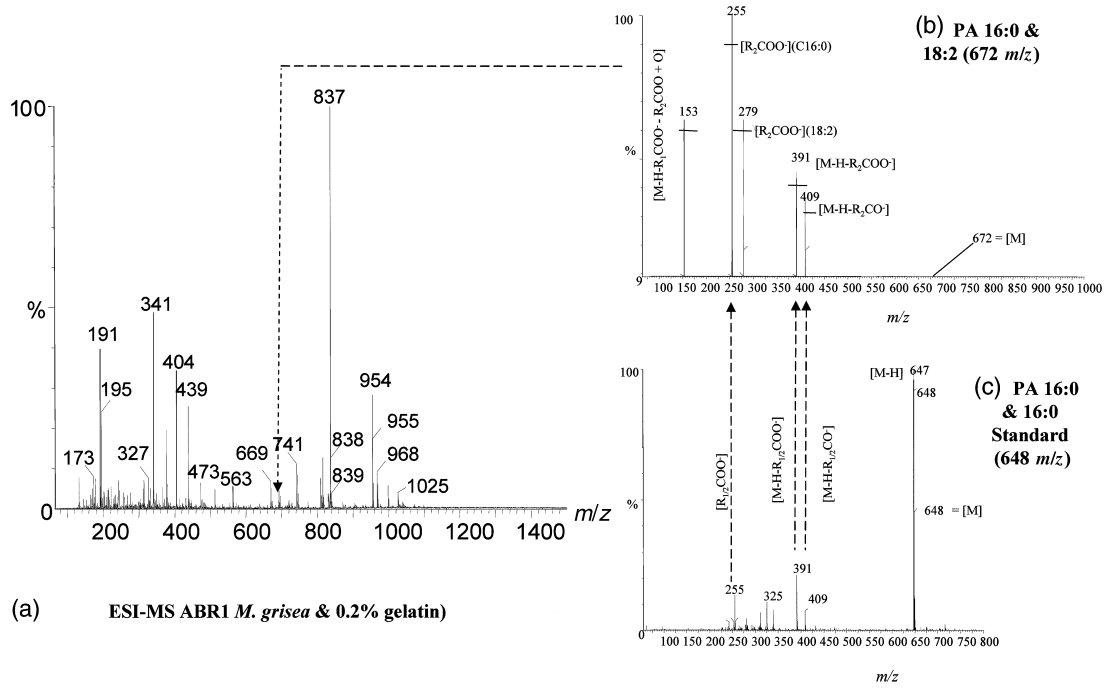

Figure 7. Negative ion mass spectra obtained by direct infusion electrospray ionization–mass spectrometry (DI-ESI-MS) of *Brachypodium distachyon* ABR1 challenged with *Magnaporthe grisea* Guy11.
(a) ESI-MS spectra of extracts of the interaction of *B. distachyon* ABR1 with *M. grisea* Guy11, and (b) ESI-MS-MS of the phosphatidic acid (PA) 16:0/18:2 (672 *m/z*) as an example of a phospholipid found to be a major source of variance (see Fig. 5 and Table 1) and (c) ESI-MS-MS of the standard PA 16:0/16:0 (648 *m/z*). Indicated are corresponding daughter ions (dotted arrows) between the standard and the deduced PA phospholipid (b).

Often, NMR and MS-based technologies are used for fingerprinting; each has advantages and disadvantages. Thus, whilst NMR is relatively insensitive (without recourse to expensive magic angle spinning or cryoprobes), unlike MS, it will not display *m/z* selectivity (Goodacre *et al.*, 2004). Our fingerprinting approach was based on FT-IR which offers low cost, high throughput and considerable chemical information (Schmitt and Flemming, 1998). However, our protocol did not include an initial quenching step but simply grinding down in water so that there could be considerable processing, both enzymatic and chemical, prior to oven-drying at 50°C, which in turn will break thermolabile bonds. Thus, the ability of FT-IR to reveal discriminatory metabolites must be necessarily limited but can be used, as in this study, to investigate variation between replicates. Nevertheless, FT-IR has been used to investigate the plant cell wall make-up and cross-linking (Séné *et al.*, 1994; Stewart *et al.*, 1995) as well as to identify cell wall mutants (Mouille *et al.*, 2003).

As with all FT-IR spectra, our results proved to be difficult to interpret visually so chemometric methods were used to analyse these data. Initially PCA was used, an unsupervised technique where inputs are clustered without *a priori* knowledge (Goodacre *et al.*, 2004). As in many studies (Goodacre *et al.*, 2003; Johnson *et al.*, 2003), PCA failed to discriminate data, which suggested that the highest variance in the sample was not associated with the factor(s) the experiment had been designed to test. As an alternative we used PC-DFA, a supervised approach where the experimental categories are known and the mathematic models are developed to attempt to match these with the input data (Goodacre *et al.*, 2004). These successfully clustered samples from *M. grisea*-challenged plants away from those from non-infected healthy and gelatine sprayed controls. Moreover, the robustness of the model was tested by validation of the clustering using different biological replicates as training and test sets. The close proximity of the projected training and test set data indicated the reproducibility of experimental conditions and thus that the *B. distachyon–M. grisea* (Guy11) pathosystem is appropriate for more detailed and costly ESI-MS analyses.

To achieve a high-throughput resolution of large numbers of metabolites, researchers using MS couple MS with a prior chromatographic (gas, liquid or high-performance liquid chromatography) step. However, technical limitations have meant that no single analytical technique may be used to profile the entire metabolome (Goodacre *et al.*, 2004). We recently demonstrated that direct infusion of plant extracts into the ESI-MS, which avoids problems associated with prior chromatography or derivatization, allowed samples from different photoperiods to be discriminated (Goodacre *et al.*, 2003), although of course isomeric metabolites cannot be resolved without chromatography.

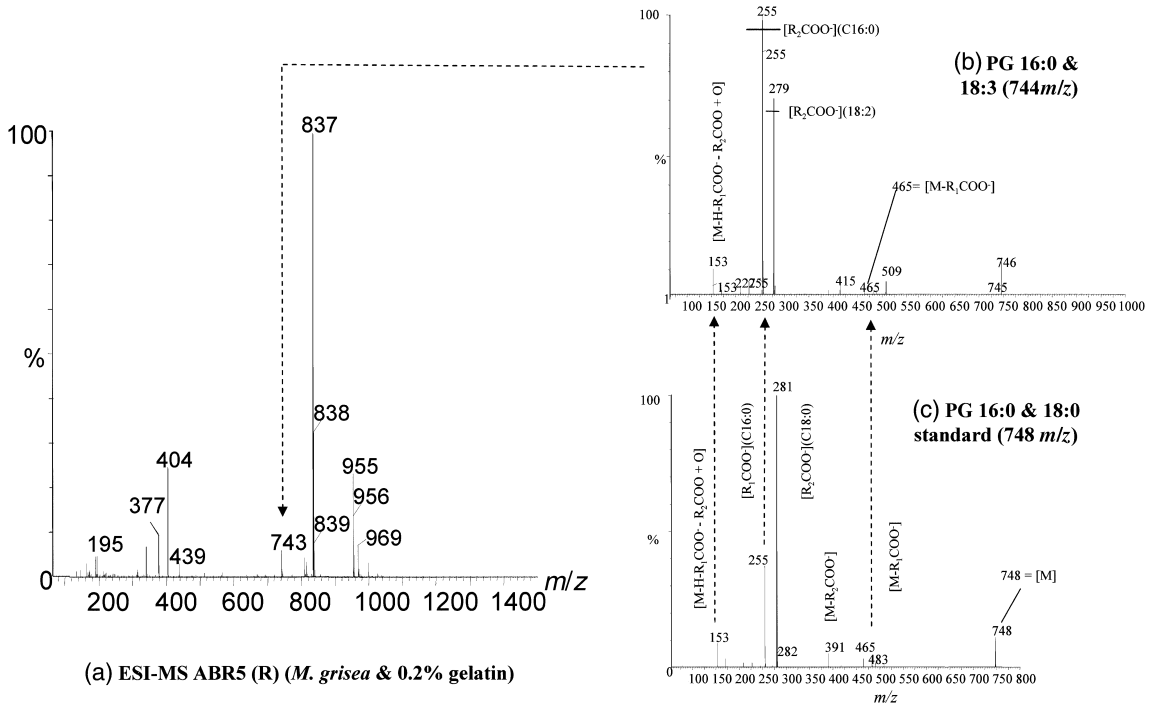

Figure 8. Negative ion mass spectra obtained by direct infusion electrospray ionization–mass spectrometry (DI-ESI-MS) of *Brachypodium distachyon* ABR5 challenged with *Magnaporthe grisea* Guy11.
(a) ESI-MS spectra of extracts of the interaction of *B. distachyon* ABR5 with *M. grisea* Guy11, and ESI MS-MS of (b) the phosphatidyl glycerol phospholipid (PG) 16:0/18:3 (744 *m/z*) as an example of a phospholipid found to be a major source of variance (see Fig. 5 and Table 1) and also of (c) the standard PG 16:0/18:0 (748 *m/z*). Indicated are corresponding daughter ions (dotted arrows) between the standard and the deduced PG phospholipid (b).

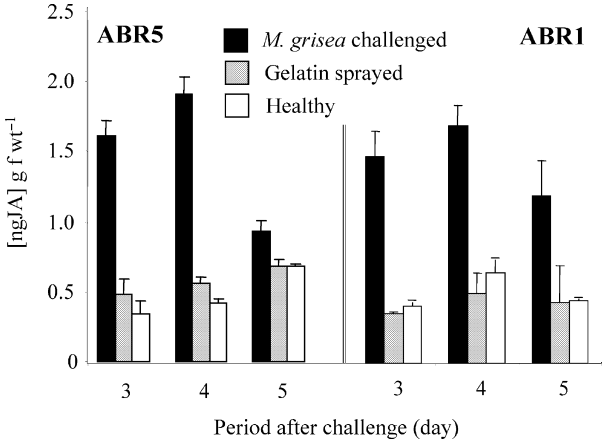

Figure 9. Accumulation of jasmonic acid in *Brachypodium distachyon* accessions following inoculation with *Magnaporthe grisea* Guy11.
Jasmonic acid levels were determined in extracts from plants of *B. distachyon* accessions ABR1 and ABR5 that were unchallenged ('healthy' □), sprayed with 0.2% gelatine ('gelatine sprayed' ▒) or challenged with *M. grisea* Guy 11 ('*M. grisea*' ■) at 3, 4, and 5 days. Levels were determined using liquid chromatography (LC)-ESI-MS and calibrated against a salicylic acid standard as described in 'Experimental procedures'. Results are given as mean ($n = 3$ replicates) JA concentration [ng JA (g FW)$^{-1}$] in the sample.

In the present study, this DI-ESI-MS approach was also successful in separately clustering metabolites from different *M. grisea* interactions with *B. distachyon* using PC-DFA. Cross-validation indicated that the derived metabolite profiles, as with FT-IR spectra of the entire metabolome, were reproducible. Chemometric analysis revealed that, within non-polar extracts, 11 analytes made the greatest contribution to the separation of resistant and susceptible material, and of challenged and gelatine-treated material.

These data reveal the following. Firstly, they indicate the high value of the *M. grisea–B. distachyon* system for obtaining metabolomic data. Given that the *B. distachyon* genome sequence is not available, this underlines the potential application of metabolomic approaches to non-sequenced model species. Secondly, and perhaps more importantly, the approach we have adopted (illustrated schematically in Figure 10) represents a rigorous method with which to derive, test and modify 'omic experiments to provide biologically meaningful data. Figure 10 illustrates two stages ('clustering and validation') where experimental parameters are tested for robustness [although the scheme omits the role of statistical considerations in the design of the first experiment(s), which is also of great importance]. Validation could occur through an examination of within-experiment variation as undertaken in this study (Figure 2D) or comparisons between experiments as in Kaplan *et al.* (2004). Crucial to the scheme is a rejection of the data if clustering or validation fails. This would necessitate a re-assessment of

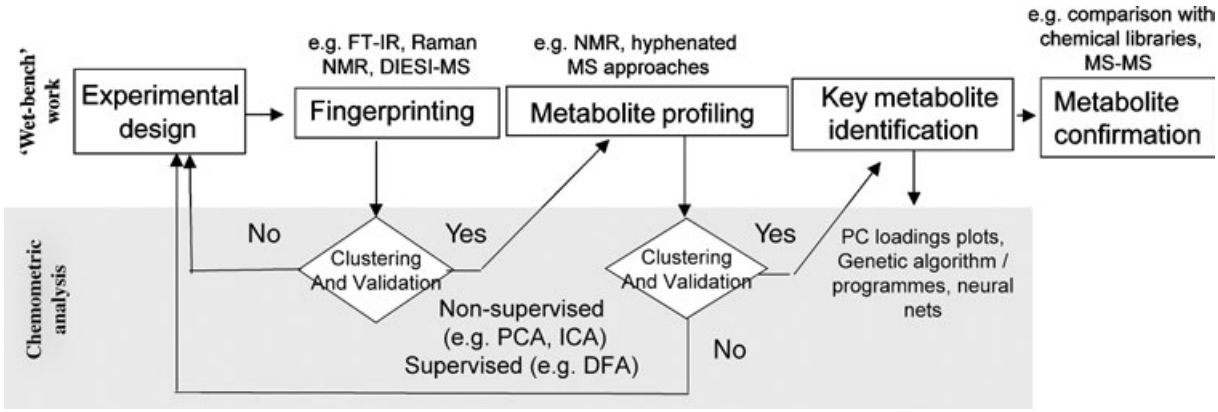

Figure 10. A schematic representation of steps undertaken in metabolomic-based analyses to validate the experimental set-up, and to select profiling and chemometric analysis methods in order to confirm metabolite identification.
A suggested metabolomic approach based on our experiences is presented. The variation which is a feature of biological experiments necessitates rigorous and statistically valid experimental design. The efficacy of the experimental design to inform the problem under investigation is assessed though a rapid and cost-effective metabolite fingerprinting approach such as Fourier-transform infrared (FT-IR) spectroscopy, Raman effect spectroscopy (RAMAN), nuclear magnetic resonance (NMR) spectroscopy or direct injection electrospray ionization mass spectrometry (DIESI-MS) and chemometric analysis such as principal component analysis (PCA) or discriminant function analysis (DFA). If the experimental approach is validated, it is appropriate to proceed to more laborious metabolite profiling using mass spectrometry (MS) with any of a range of pre-separation techniques or DIESI-MS. The results should again be validated by chemiometric approaches. Key metabolites could be identified by either examination of PC-loading plots and confirmation by tandem MS (MS-MS, as in this paper), pattern recognition by genetic algorithms/programs or direct comparison with pre-existing spectral libraries.

the experimental design, extraction method or detection technique.

Distinct phospholipid changes are associated with disease development and resistance in the M. grisea–B. distachyon *interaction*

To begin to characterize the metabolite changes that contributed most to the variation seen in *B. distachyon* interactions with *M. grisea*, we chose to focus on profiling non-polar sample extracts for the reasons already stated, and also because our earlier investigations had suggested that phospholipid-derived oxylipins were relevant defence signals in the *M. grisea–B. distachyon* Guy11 interaction (Mur *et al.*, 2004). It should also be stressed that our aim was not an exhaustive, global determination of the *M. grisea*-challenged *B. distachyon* metabolome but a demonstration that metabolomic approaches can be used to investigate a highly heterogeneous and dynamic biological scenario.

Plant fatty acid synthesis occurs leading to the synthesis of palmitic acid (C16:0) or oleic acid (C18:1), which when linked to acyl carrier protein (ACP) can enter glycerolipid synthesis to form diglycerides (PLs) or triglycerides which are major storage lipids (reviewed by Ohlrogge and Browse, 1995). Desaturation of steric acid (C18:0) to form oleic acid is carried out by a stearoyl-ACP desaturase (encoded by *FAD2*/*SSI2*) which regulates the levels of unsaturated fatty acid levels within the cell. Glycerol-3-phosphate (G3P) is transferred to the acyl chain by G3P acyl transferase encoded by *ACT1*. This produces lysophophatidic acid (LPA, a monoacylglycerol) to which a second acyl chain in transferred via LPA-acyl transferase to form PA. The acyl chain may be modified by other desaturases and a range of head groups may be attached (Ohlrogge and Browse, 1995). Arabidopsis *ssi2* mutant plants exhibit reduced C18:1 levels and concomitant activation of the defence-associated salicylic acid (SA)-mediated defence pathway and suppression of JA signalling (Kachroo *et al.*, 2001). The phenotype of the *ssi2* mutation can be rescued by introgression into an *act1* mutation which reduces C18:1 flux into glycerolipid synthesis, suggesting that the levels of C18:1 are important in the regulation of SA and JA signalling cascades (Kachroo *et al.*, 2004).

Other defence signalling mechanisms involve differential processing of PLs (reviewed by Meijer and Munnik, 2003; see also Figure 6). Perhaps the best-studied PL signalling pathway involves a minor membrane PL with an inositol head group, phosphatidylinositol-2-phosphate (PIP_2) (<0.1% of total). In phosholipase C (PLC), removal of the polar head group (Figure 6) produces soluble inositol triphosphate (IP_3) signals which are involved in calcium mobilization, whilst the residual diacylglycerol (DAG), which remains in the membrane, activates the protein kinase C super family. In plants, addition of defence elicitors to tomato cells resulted in a PLC-mediated hydrolysis of PIP_2 which subsequently induced a transient rise in phosphatidic acid (PA), which was generated from DAG by a DAGkinase (van Der Luit *et al.*, 2000; Munnik, 2001). In tobacco (*Nicotiana tabacum*), specific increases in PA and DAG were noted following defence elicitation (de Jong *et al.*, 2004). PA was generated directly either by phospholipase D (PLD) or PLC-mediated cleavage followed by phosphorylation of DAG (Figure 6). Increases in PA in both tomato and Arabidopsis have been linked to the initiation of ROS generation, a central event in plant

resistance (de Jong *et al.*, 2004; Sang *et al.*, 2001; Zhang *et al.*, 2003).

Our metabolite profiles indicated that PA PLs but not PG PLs exhibited differential accumulation in ABR1 compared with ABR5 following infection with *M. grisea*. It is important to emphasize that this did not reflect basic variation in membrane lipids between the two accessions but represented differential responses to fungal challenge. The challenged background was subtracted from the unchallenged background for each accession separately, and hence only metabolite pathogen-induced metabolite variance was targeted. Accessions ABR1 and ABR5 originate from different geographical locations (Routledge *et al.*, 2004) and undoubtedly harbour considerable genetic and metabolite heterogeneity. Indeed, Figure 4 reveals that the variance between the two accessions when unchallenged is as great as the variance between challenged and unchallenged material within each accession. Comparisons (not shown) of the mean ($n = 10$ biological replicates) mass intensities of targeted *m/z* ions in both unchallenged ABR1 and ABR5 showed that basic differences in membrane composition were seen with PG PLs, with levels being higher in ABR5. An examination (not shown) of spectra from fungal cultures revealed that only one ion (439 *m/z*) was common between the fungus and plant. Therefore, the discriminatory PA PLs were not derived from the fungus unless they accumulated only during plant infection. We consider that this was unlikely, as we found no evidence of major fungal non-polar metabolites such as ergosterol or arachidonic acid being targeted as discriminatory ions in pathogen-challenged as compared with unchallenged samples. Taking all of these points into consideration, PAs emerge as significant metabolites in the response of *B. distachyon* to *M. grisea*. However, it was difficult to relate our data to either resistance or susceptibility, as PAs were not uniformly raised or lowered in either accession. Although only ABR5 exhibited a detectable oxidative burst in response to *M. grisea* (Routledge *et al.*, 2004), increases of individual PAs were seen in both accessions. This could indicate a high level of specificity in PA-mediated defences, so that only PA with specific acyl tails eliciting defences and/or fungal intervention modifies any inducing action. To address such questions fully requires carefully targeted biochemical analysis (e.g. de Jong *et al.*, 2004) and mutational studies (e.g. Kachroo *et al.*, 2001, 2004) for which *B. distachyon* could be a suitable model (Draper *et al.*, 2001). Equally, biochemical studies assessing processes such as differential phospholipase activity would be appropriate.

In mammalian systems, removal of fatty acyl chains by either phospholipase A_1 or A_2 leads to the formation of eicosanoids. In plants, the derivation of a PL-derived acyl chain, linolenic acid (C18: 3), leads to the formation of oxylipins such as JA (Blee, 2002). Phosphatidylglycerolipids are the major PL class found in plant chloroplasts (Marechal *et al.*, 1997). In tomato, the *spr2* mutation proved to be within a fatty acid desaturase, ultimately required for the production of oxylipins such as JA. SPR2 proved to have a specificity for chloroplast PLs which, given the preponderance of PG, suggests that these are major sources of JA in tomato. Assuming that this is also the case for *B. distachyon*, the significant reduction of PG PLs in both accessions could indicate that these are the source of oxylipin generation. As PGs were reduced in both accessions following challenge with *M. grisea*, we predicted that JA levels would increase and indeed this proved to be the case (Figure 10).

Montillet *et al.* (2004) recently profiled oxylipin products produced in Arabidopsis as a result of oxidative stress elicited by the bacterial protein harpin using HPLC and also ESI-MS. Comparisons with control plants yielded a range of lipophillic polyunsaturated fatty acid hydroperoxides. Although non-polar solvents were used in the Montillet *et al.* study (chloroform) and in our study (propan-2-ol), our chemometric analyses did not target lipid hydroperoxides, or indeed JA, as being discriminatory between *M. grisea*-challenged ABR1 and ABR5. Examination of the subtraction spectra indicated increases in the *m/z* ion corresponding to JA following challenge with *M. grisea* but the differences were of marginal significance ($P = 0.017$). Clearly, such an observation was at odds with data presented in Figure 10 using a targeted metabolite profiling approach. This highlights the need for multiple sample extraction approaches, and possibly detection technologies, in order to approach the goal of a global metabolite profile.

In conclusion, our study has demonstrated the potential of metabolomics to reveal discriminatory metabolites within a highly heterogeneous system. Our highlighting of different PL groups has generated biologically relevant hypotheses through inductive means which will now be examined by more targeted approaches. Equally, our results highlight some remaining problems, particularly the need to use a wide variety of extraction techniques and probably detection technologies in order to allow a full metabolome to be generated.

Experimental procedures

Organisms, cultivation, and infection procedure

Magnaporthe grisea Guy11 was cultured on potato dextrose agar (PDA) at 24°C for 2 weeks. After sporulation, spores were removed from the surface of the plate with a glass-spreader and suspended in 0.2% gelatine solution. The spore solution was applied to 3–4-week-old *B. distachyon* ABR1 and ABR5 plants (long day 12–16 h; 1×400 W high-pressure sodium plant irradiating bulb; 23 ± 2°C) using an airbrush. Untreated and 0.2% gelatine-sprayed controls were also prepared for both the ABR1 and ABR5 accessions.

Brachypodium distachyon accessions ABR1 and ABR5 were bagged to maintain humidity which allowed infection to take place. The plants were then placed in a Fisons Fi-totron 600-H growth

cabinet (30°C, 9.5 h light, 50–80% humidity, 80 μM m^2 sec^{-1} light intensity). After 24 h, the bags were removed and the *B. distachyon* plants were watered every 24 h until harvest (72 h after removal of bags). Visualization of *in planta* fungal development by alanine blue staining is described in Routledge *et al.* (2004).

Fourier-transform infrared (FT-IR) spectroscopy

Sampled plant material [approximately 100 mg fresh weight (FW)] was immediately ground in a mortar and pestle in 1 ml of water without any prior processing, and 15 μl of the sample homogenate was loaded onto a 100-well aluminium sample plate (Ellis *et al.*, 2003). Each biological replicate was loaded six times onto a single FT-IR plate and this was repeated on a further two plates ('machine' replicates). The plates were oven-dried at 50°C for 30 min before being loaded into the scanning compartment of a Bruker IFS28 infrared spectrometer (Bruker Ltd, Coventry, UK) and FT-IR spectra obtained as described elsewhere (Goodacre *et al.*, 1998; Johnson *et al.*, 2003).

Electrospray ionization mass spectrometry (ESI-MS) harvest and extraction

The most diseased leaves were selectively harvested and samples (approximately 30 mg FW) were placed into 2-ml microcentrifuge tubes, each containing a single stainless-steel ball. Samples were then frozen in N_2 liquid and stored at −80°C for no more than 1 week. The extraction procedure essentially followed that of Fiehn *et al.* (2000), except that only the non-polar phase was sampled. A chloroform, methanol and water-based solvent mixture (at a ratio of 1:2.5:1) was used as the extraction buffer. The sample extracts were centrifuged, and the solvent phase was removed and then dried down in a speed vacuum. Samples were reconstituted in propan-2-ol (70%) and water (30%) for analysis. Acetonitrile and methanol were also tested, although 70% propan-2-ol produced the spectra with the greatest signal-to-noise ratio.

ESI-MS analysis

Metabolomic analysis of the highly polar lipid and PL extracts was carried out using ESI-MS on a Micromass LCT mass spectrometer (Waters, Manchester, UK). Spectra were collected in the negative ionization mode (ES^-). Samples were introduced into the electrospray source by direct infusion at a flow rate of 5 μl min^{-1}, using a Harvard11 syringe pump (Harvard Apparatus Inc., Holliston, MA, USA).

To optimize spectral collection, the sample cone voltage was increased sequentially to 30, 40, 60, 80, and 100 V while maintaining the extraction cone voltage at 5 V. The optimum cone voltage was found to be 30 V. The capillary voltage was set at −2.2 kV, the source and desolvation temperatures were 80 and 100°C, respectively, and the desolvation and nebulizer gas flow rates were 400 l h^{-1} and 50 l h^{-1}, respectively.

A mass resolution of 4500 (FWHM, full width half maximum) was achieved by using an LCT instrument which employed a reflectron time-of-flight (re-ToF) mass analyser (Guilhaus *et al.*, 1997). Data were acquired over the *m/z* range 65–1400 Th.

Tandem MS (ESI-MS-MS)

Tandem MS was performed on a Micromass Q-ToF (Waters, Manchester, UK) using the same protocol as detailed above; the aspects of the procedure that differed were as follows. The flow rate was 8 μl min^{-1} via a 250-μl Hamilton syringe; the nebulizer gas flow rate was 20 l h^{-1}; the desolvation flow rate was 375 l h^{-1}. Data were acquired over the *m/z* range 55–1000 Th. Argon was used as the collision gas. At an inlet pressure of 12 psi, the analyser\collision cell penning gauge reading was 2.8 e-5 mBar. Selected precursor irons underwent low energy collision induced dispersal (CID) with greater collision energy (c\e) used with increasing *m/z*. Thus, with *m/z* ranging from 650 to 720 Th, a c\e of 30 V was used, for 720 to 800 Th a c\e of 35 V and for *m/z* >800 a a c\e of 55 V. To confirm that the identified metabolites were PA and PG PLs, standards had to be run in ESI-MS. 1,2-Dipalmitoyl-sn-glycero-3-phosphate sodium salt and 1-palmitoyl-2-oleoyl-sn-glycero-3-phospho-rac-(1-glycerol) ammonium salt standards were obtained from Sigma-Aldrich Company Ltd (Gillingham, UK) for this purpose. PL standards were also run following the same protocol.

Liquid chromatography–mass spectrometry (LC-MS)

Samples were reconstituted in H_2O:CH_3OH (5:95). An isocratic column solvent solution was prepared [H_2O:NaOAc (in CH_3OH) (5:95)] and all solvents were HPLC grade. Samples (10 μl) were injected onto a 2.1 × 50 mm Waters Symmetry C^{18} column (Waters, Milford, MA, USA) at a flow rate of 0.15 ml min^{-1} with no split. Sample and column temperatures were 12 and 25°C, respectively.

MS was undertaken using a Micromass Ltd Q-ToF in negative (ES^-) ion mode at −2.0 kV. The sample cone voltage was set to 60 V and the extraction cone voltage to 5 V. The source and desolvation temperatures were 120 and 250°C, respectively, and the desolvation and nebulizer gas flow rates were 400 and 20 l h^{-1} (no purge), respectively. Data were acquired over the *m/z* range 65–1000 Th, and the acquisition time was one spectrum every 1.9 sec, with an inter-acquisition period of 0.1 sec. Argon was used as the collision gas, with a c/e of 55 V. At an inlet pressure of 12 psi, the analyser/collision cell penning gauge reading was 3.2 e^{-5} mBar.

Cluster analysis

The FT-IR and ESI-MS spectra that were obtained were exported in ASCII format from instrument manufacturers' software and imported into MATLAB version 6.5 (The MathWorks Inc., Natwick, MA, USA). MATLAB runs under Microsoft Windows NT on an IBM-compatible PC.

The spectra were pre-processed as follows. For FT-IR data, the first derivative spectra were calculated using the Savitzky–Golay algorithm with five-point smoothing (Savitzky and Golay, 1964). For ESI-MS, the data were binned to unit mass and then normalized to percentage total ion count.

The data were first analysed using principal components analysis (PCA; Causton, 1987) according to the NIPALS algorithm (Wold, 1966). Briefly, this involves projecting a ('X') matrix formed from set of (*N*) spectra with a given mass range (*p*) (i.e. a $N \times p$ matrix) onto multidimensional space. Principal components (PCs) are linear combinations of original variables (known as loadings) which are used in the projection of the X matrix. Individual PCs are ranked (PC1, PC2, etc.) on the basis of the variance within the original dataset that is explained. PCA is an unsupervised method where no *a priori* knowledge of experimental structure is given. Thus, if there is clustering of either 2D or 3D projections of PCA from replicate data, this indicates that the original experimental parameters are the sources of maximal variation. PCA was followed by discriminant function analysis (DFA) which is a supervised projection method (Manly, 1994). DFA then discriminated between groups on the basis of the retained PCs and the *a priori* knowledge of which spectra were replicates (either biological or machine). DFA was programmed to

maximize the Fisher ratio (i.e. the within-class to between-class variance) and the spectral similarity between different classes reflects the optimal number of PCs that are fed into the DFA algorithm. All calculations were performed in MATLAB.

Cluster analysis validation

In order to validate the cluster analysis, ten biological replicates of each experimental class were collected. Eight of the ten replicates were selected randomly to produce PC-DFA, where DFA was programmed with the first 20 PCs and *a priori* knowledge of plant groups. Subsequently the two remaining spectra were then projected into the PC-DFA ordinate space, as described elsewhere (Jarvis and Goodacre, 2004).

Further cluster analysis on ESI-MS data was carried out on the gelatine-treated and infected material of the ABR1 and ABR5 accessions individually. For both accessions, a subtraction of gelatine-treated from infected mean averaged spectra revealed the ions contributing to the differences between infected and gelatine-treated material. These ions were then compared with a plot of the DFA loading vectors against *m/z*. Ions that significantly contributed to the DFA loading vectors and that were also present in the subtraction spectra were assumed to be substances involved in the fungal reprogramming of the host metabolome or the resistance of the plant to the fungus. These substances were tentatively identified as PLs according to *m/z*, and were used as targets for ESI-MS-MS confirmation.

Measurements of jasmonic acid levels

The plant material was extracted and analysed on a Micromass LCT ESI-MS (Waters Ltd, Manchester, UK) as described in Clarke *et al.* (2004). JA levels were calculated from the recovery of JA against an added d_6-SA standard. Differences in the recovery of JA as opposed to SA (which the assay was originally designed to determine) meant that calibration was required. Thus, a JA standard (Sigma JA standard J2 750) was serially diluted and added to a set volume of d_6-SA and analysed on the LCT ESI-MS. A JA standard curve was calculated by plotting the measured JA:d_6-SA (*m/z*) ratio against the given JA:d_6-SA molar ratio. Calibration against d_6-SA indicated that the analysis was approximately 10-fold less sensitive for JA than it was for SA. JA in the plant material was then quantified by calibration of the molar ratio between the $[M\text{-}H]^-$ ions at *m/z* 210 (JA) and *m/z* 141 (d_6-SA internal standard), and calibrated against the standard curve molar ratio, to give a true concentration.

Acknowledgements

We wish to thank Drs Helen Johnson (Manchester, UK), Ian Scott and Jacqueline Wood (both Aberystwyth, UK) for their help and advice with the data described in this paper. Gemma Bell provided the alanine blue material to reveal *in planta* fungal development. Plant material was grown and maintained by Pat Causton, Tom Thomas and Ray Smith (Aberystwyth, UK). *Magnaporthe grisea* strain Guy11 was the kind gift of Professor Nick Talbot (Exeter, UK). JWA is supported by a UK BBSRC committee studentship. RG is also indebted to the UK BBSRC for financial support. All pathogen work is carried out under DEFRA licence PHL 123A/4324.

Supplementary Material

The following supplementary material is available for this article online:

Figure S1. Mass spectra of *Magnaporthe grisea*-challenged plants and controls of *Brachypodium distachyon* ecotypes ABR1 and ABR5.

Example mass spectra for *B. distachyon* ecotypes (A) ABR1 (susceptible) and (B) ABR5 (resistant) challenged with *M. grisea* strain Guy 11 0.2% gelatine, treated with 0.2% gelatine alone or untreated are shown. Spectra are equilibrated to the maximum ion intensities. Relative ion intensities are given for each spectrum. Several of the metabolites that were found to be discriminatory between ecotypic responses to pathogenic challenge (e.g. *m/z* 670, 720, 742, 744, 816 and 838; see main text and Table 1) are particularly prominent. To illustrate the richness of *m/z* in the spectra, details of the 300–500 *m/z* region (shaded) are given, again equilibrating to maximum ion intensities. This region describes much of the variation seen attributable to ecotype and responses to 0.2% gelatine (see main text and Figures 4 and 5). Some major sources of such variance (identified in PC-DF1 loading spectra; see Figure 4) are annotated and indicated in red.

This material is available as part of the online article from http://www.blackwell-synergy.com

References

Baker, B., Zambryski, P., Staskawicz, B. and Dinesh-Kumar, S.P. (1997) Signaling in plant-microbe interactions. *Science*, **276**, 726–733.

Balhadere, P.V. and Talbot, N.J. (2001) PDE1 encodes a P-type ATPase involved in appressorium-mediated plant infection by the rice blast fungus *Magnaporthe grisea*. *Plant Cell*, **13**, 1987–2004.

Bino, R.J., Hall, R.D., Fiehn, O. *et al.* (2004) Potential of metabolomics as a functional genomics tool. *Trends Plant Sci.* **9**, 418–425.

Blee, E. (2002) Impact of phyto-oxylipins in plant defense. *Trends Plant Sci.* **7**, 315–322.

Brugger, B., Erben, G., Sandhoff, R., Wieland, F.T. and Lehmann, W.D. (1997) Quantitative analysis of biological membrane lipids at the low picomole level by nano-electrospray ionization tandem mass spectrometry. *Proc. Natl Acad. Sci. USA*, **94**, 2339–2344.

Causton, D.R. (1987) *A Biologist's Advanced Mathematics*. London: Allen and Unwin.

Choi, Y.H., Tapias, E.C., Kim, H.K., Lefeber, A.W., Erkelens, C., Verhoeven, J.T., Brzin, J., Zel, J. and Verpoorte, R. (2004) Metabolic discrimination of *Catharanthus roseus* leaves infected by phytoplasma using 1H-NMR spectroscopy and multivariate data analysis. *Plant Physiol.* **135**, 2398–2410.

Clarke, S.M., Mur, L.A.J., Wood, J.E. and Scott, I.M. (2004) Salicylic acid dependent signaling promotes basal thermotolerance but is not essential for acquired thermotolerance in *Arabidopsis thaliana*. *Plant J.* **38**, 432–447.

van Der Luit, A.H., Piatti, T., van Doorn, A., Musgrave, A., Felix, G., Boller, T. and Munnik, T. (2000) Elicitation of suspension-cultured tomato cells triggers the formation of phosphatidic acid and diacylglycerol pyrophosphate. *Plant Physiol.* **123**, 1507–1516.

Draper, J., Mur, L.A.J., Jenkins, G., Ghosh-Biswas, G.C., Bablak, P., Hasterok, R. and Routledge, A.P. (2001) *Brachypodium distachyon*: a new model system for functional genomics in grasses. *Plant Physiol.* **127**, 1539–1555.

Dunn, W.B. and Ellis, D.I. (2005) Metabolomics: current analytical platforms and methodologies. *Trends Analyt. Chem.* **24**, 285–294.

Ellis, D.I., Harrigan, G.G. and Goodacre, R. (2003) Metabolic fingerprinting with Fourier transform infrared spectroscopy. In *Metabolic Profiling: Its Role in Biomarker Discovery and Gene Function Analysis* (Harrigan, G.G. and Goodacre, R., eds). Boston, MA: Kluwer Academic Publishers, pp. 111–124.

Fang, J. and Barcelona, M.J. (1998) Structural determination and quantitative analysis of bacterial phospholipids using liquid chromatography/electrospray ionisation/mass spectrometry. *J. Microbiol. Methods* **33**, 23–35.

Fiehn, O. (2001) Combining genomics, metabolome analysis, and biochemical modelling to understand metabolic networks. *Comp. Funct. Genomics*, **2**, 155–168.

Fiehn, O. (2002) Metabolomics-the link between genotypes and phenotypes. *Plant Mol. Biol.* **48**, 155–171.

Fiehn, O. and Weckwerth, W. (2003) Deciphering metabolic networks. *Eur. J. Biochem.* **270**, 579–588.

Fiehn, O., Kopka, J., Dormann, P., Altmann, T., Trethewey, R.N. and Willmitzer, L. (2000) Metabolite profiling for plant functional genomics. *Nat. Biotechnol.* **18**, 1157–1161.

Foster, A.J., Jenkinson, J.M. and Talbot, N.J. (2003) Trehalose synthesis and metabolism are required at different stages of plant infection by *Magnaporthe grisea*. *EMBO J.* **22**, 225–235.

Goodacre, R. (2003) Explanatory analysis of spectroscopic data using machine learning of simple, interpretable rules. *Vibrational Spectrosc.* **32**, 33–45.

Goodacre, R. (2005) Making sense of the metabolome using evolutionary computation: seeing the wood with the trees. *J. Exp. Bot.* **56**, 245–254.

Goodacre, R., Timmins, E.M., Burton, R., Kaderbhai, N., Woodward, A.M., Kell, D.B. and Rooney, P.J. (1998) Rapid identification of urinary tract infection bacteria using hyperspectral whole-organism fingerprinting and artificial neural networks. *Microbiology*, **144**, 1157–1170.

Goodacre, R., Heald, J.K. and Kell, D.B. (1999) Characterisation of intact microorganisms using electrospray ionisation mass spectrometry. *FEM Microbiol. Lett.* **176**, 17–24.

Goodacre, R., Vaidyanathan, S., Bianchi, G. and Kell, D.B. (2002) Metabolic profiling using direct infusion electrospray ionisation mass spectrometry for the characterisation of olive oils. *Analyst*, **11**, 1457–1462.

Goodacre, R., York, E.V., Heald, J.K. and Scott, I.M. (2003) Chemometric discrimination of unfractionated plant extracts profiled by flow-injection electrospray mass spectrometry. *Phytochemisty*, **62**, 859–863.

Goodacre, R. Vaidyanathan, S., Dunn, W.B., Harrigan, G.G. and Kell, D.B. (2004) Metabolomics by numbers – acquiring and understanding global metabolite data. *Trends Biotechnol.* **22**, 245–252.

van der Greef, J., Stroobant, P. and van der Heijden, R. (2004) The role of analytical sciences in medical systems biology. *Curr. Opin. Chem. Biol.* **8**, 559–565.

Griffin, J.L. (2003) Metabolomics: NMR spectroscopy and pattern recognition analysis of body fluids and tissues for characterisation of xenobiotic toxicity and disease diagnosis. *Curr. Opin. Chem. Biol.* **7**, 648–664.

Guilhaus, M., Mlynski, V. and Selby, D. (1997) Perfect timing: time-of-flight mass spectrometry. *Rapid Comm Mass Spectrom*, **11**, 951–962.

Gygi, S.P., Rochon, Y., Franza, B.R. and Aebersold, R. (1999) Correlation between protein and mRNA abundance in yeast. *Mol. Cell. Biol.* **19**, 1720–1730.

Hall, R., Beale, M., Fiehn, O., Hardy, N., Sumner, L. and Bino, R. (2002) Plant metabolomics: the missing link in functional genomic strategies. *Plant Cell*, **14**, 1437–1440.

Hirai, M.Y., Yano, M., Goodenowe, D.B., Kanaya, S., Kimura, T., Awazuhara, M., Arita, M., Fujiwara, T. and Saito, K. (2004) Integration of transcriptomics and metabolomics for understanding of global responses to nutritional stresses in *Arabidopsis thaliana*. *Proc. Natl Acad. Sci. USA*, **101**, 10205–10210.

Jarvis, R.M. and Goodacre, R. (2004) Rapid discrimination of bacteria using surface enhanced Raman spectroscopy. *Anal. Chem.* **76**, 40–47.

Johnson, H.E., Broadhurst, D., Goodacre, R. and Smith, A.R. (2003) Metabolic fingerprinting of salt-stressed tomatoes. *Phytochemistry*, **62**, 919–928.

de Jong, C.F., Laxalt, A.M., Bargmann, B.O., de Wit, P.J., Joosten, M.H. and Munnik, T., (2004) Phosphatidic acid accumulation is an early response in the *Cf-4/Avr4* interaction. *Plant J.* **39**, 1–12.

Kachroo, P., Shanklin, J., Shah, J., Whittle, E.J. and Klessig, D.F. (2001) A fatty acid desaturase modulates the activation of defense signaling pathways in plants. *Proc. Natl Acad. Sci. USA*, **98**, 9448–9453.

Kachroo, A., Venugopal, S.C., Lapchyk, L., Falcone, D., Hildebrand, D. and Kachroo, P. (2004) Oleic acid levels regulated by glycerolipid metabolism modulate defense gene expression in *Arabidopsis*. *Proc. Natl Acad. Sci. USA*, **101**, 5152–5157.

Kaderbhai, N.N., Broadhurst, D.I., Ellis, D.I., Goodacre, R. and Kell, D.B. (2003) Functional genomics via metabolic footprinting: monitoring metabolite secretion by *Escherichia coli* tryptophan metabolism mutants using FT–IR and direct injection electrospray mass spectrometry. *Comp. Funct. Genomics*, **4**, 376–391.

Kaplan, F., Kopka, J., Haskell, D.W., Zhao, W., Schiller, K.C., Gatzke, N., Sung, D.Y. and Guy, C.L. (2004) Exploring the temperature-stress metabolome of *Arabidopsis*. *Plant Physiol.* **136**, 4159–4168.

Kawasaki, T., Henmi, K., Ono, E., Hatakeyama, S., Iwano, M., Satoh, H. and Shimamoto, K. (1999) The small GTP-binding protein rac is a regulator of cell death in plants. *Proc. Natl Acad. Sci. USA*, **96**, 10922–10926.

Kell, D.B. and Oliver, S.G. (2004) Here is the evidence, now what is the hypothesis? The complementary roles of inductive and hypothesis-driven science in the post-genomic era. *Bioessays*, **26**, 99–105.

Kim, S., Ahn, I.P. and Lee, Y.H. (2001) Analysis of genes expressed during rice-*Magnaporthe grisea* interactions. *Mol. Plant Microbe Interact.* **14**, 1340–1346.

Lee, M.W., Qi, M. and Yang, Y. (2001) A novel jasmonic acid-inducible rice myb gene associates with fungal infection and host cell death. *Mol. Plant Microbe Interact.* **14**, 527–535.

Manly, B.F.J. (1994) *Multivariate Statistical Methods: A Primer*. London: Chapman Hall.

Mann, M. and Jensen, O.N. (2003) Proteomic analysis of post-translational modifications. *Nat. Biotechnol.* **21**, 255–261.

Marechal, E., Block, M.A., Dorne, A.-J. and Joyard, J. (1997) Lipid synthesis and metabolism in the plastid envelope. *Plant Physiol.* **100**, 65–77.

Matsumura, H., Reich, S., Ito, A., Saitoh, H., Kamoun, S., Winter, P., Kahl, G., Reuter, M., Kruger, D.H. and Terauchi, R. (2003) Gene expression analysis of plant host-pathogen interactions by SuperSAGE. *Proc. Natl Acad. Sci. USA*, **100**, 15718–15723.

Meijer, H.J. and Munnik, T. (2003) Phospholipid-based signaling in plants. *Annu. Rev. Plant Biol.* **54**, 265–306.

Montillet, J.L., Cacas, J.L., Garnier, L. *et al.* (2004) The upstream oxylipin profile of *Arabidopsis thaliana*: a tool to scan for oxidative stresses. *Plant J.* **40**, 439–451.

Mouille, G., Robin, S., Lecomte, M., Pagant, S. and Hofte, H. (2003) Classification and identification of *Arabidopsis* cell wall mutants using Fourier-Transform InfraRed (FT-IR) microspectroscopy. *Plant J.* **35**, 393–404.

Munnik, T. (2001) Phosphatidic acid: an emerging plant lipid second messenger. *Trends Plant Sci.* **6**, 227–233.

Mur, L.A.J., Xu, R., Casson, S.A., Stoddart, W.M., Routledge, A.P. and Draper, J. (2004) Characterization of a proteinase inhibitor

from *Brachypodium distachyon* suggests the conservation of defence signalling pathways between dicotyledonous plants and grasses. *Mol. Plant Pathol.* **5**, 267–280.

Narasimhan, K., Basheer, C., Bajic, V.B. and Swarup, S. (2003) Enhancement of plant-microbe interactions using a rhizosphere metabolomics-driven approach and its application in the removal of polychlorinated biphenyls. *Plant Physiol.* **132**, 146–153.

Nelson, A.J., Doerner, P.W., Zhu, Q. and Lamb, C.J. (1994) Isolation of a monocot 3-hydroxy-3-methylglutaryl coenzyme A reductase gene that is elicitor-inducible. *Plant Mol. Biol.* **25**, 401.

Ohlrogge, J. and Browse, J. (1995) Lipid biosynthesis. *Plant Cell*, **7**, 957–970.

Ono, E., Wong, H.L., Kawasaki, T., Hasegawa, M., Kodama, O. and Shimamoto, K. (2001) Essential role of the small GTPase Rac in disease resistance of rice. *Proc. Natl Acad. Sci. USA*, **98**, 759–764.

Ou, S.H. (1985) *Rice Diseases*. Kew, Surrey: Commonwealth Mycological Institute CAB.

Pickersky, E. and Gang, D.R. (2000) Genetics and biochemistry of secondary metabolites: an evolutionary perspective. *Trends Plant Sci.* **5**, 439–445.

Raamsdonk, L.M., Teusink, B., Broadhurst, D. *et al.* (2001) A functional genomics strategy that uses metabolome data to reveal the phenotype of silent mutations. *Nat. Biotechnol.* **19**, 45–50.

Rauyaree, P., Choi, W., Fang, E., Blackmon, B. and Dean, R. (2001) Genes expressed during early stages of rice infection with the rice blast fungus *Magnaporthe grisea*. *Mol. Plant Pathol.* **2**, 347–354.

Redman, J.C., Haas, B.J., Tanimoto, G. and Town, C.D. (2004) Development and evaluation of an *Arabidopsis* whole genome Affymetrix probe array. *Plant J.* **38**, 545–561.

Roessner, U., Luedemann, A., Brust, D., Fiehn, O., Linke, T., Willmitzer, L. and Fernie, A. (2001) Metabolic profiling allows comprehensive phenotyping of genetically or environmentally modified plant systems. *Plant Cell*, **13**, 11–29.

Routledge, A.P., Shelley, G., Smith, J.V., Talbot, N.J., Draper, J. and Mur, L.A.J. (2004) *Magnaporthe grisea* interactions with the model grass *Brachypodium distachyon* closely resemble those with rice (*Oryza sativa*). *Mol. Plant Pathol.* **5**, 253–265.

Sang, Y., Cui, D. and Wang, X. (2001) Phospholipase D and phosphatidic acid-mediated generation of superoxide in *Arabidopsis*. *Plant Physiol.* **126**, 449–458.

Savitzky, A. and Golay, M.J.E. (1964) Smoothing and differentiation of data by simplified least squares procedures. *Anal. Chem.* **36**, 1627–1633.

Schmitt, J. and Flemming, H.C. (1998) FT-IR-spectroscopy in microbial and material analysis. *Int. Biodeterior. Biodegradation*, **41**, 1–12.

Schweizer, P., Buchala, A. and Metraux, J.P. (1997) Gene-expression patterns and levels of jasmonic acid in rice treated with the resistance inducer 2, 6-dichloroisonicotinic acid. *Plant Physiol.* **115**, 61–70.

Séné, C., McCann, M.C., Wilson, R.H. and Grinter, R. (1994) Fourier-Transform Raman and Fourier-Transform Infrared Spectroscopy (An investigation of five higher plant cell walls and their components). *Plant Physiol.* **106**, 1623–1631.

Shim, K.S., Cho, S.K., Jeung, J.U. *et al.* (2004) Identification of fungal (*Magnaporthe grisea*) stress induced genes in wild rice (*Oryza minuta*). *Plant Cell Rep.* **22**, 599–607.

Stewart, D., Wilson, H.M., Hendra, P.J. and Morrison, I. (1995) Fourier-Transform Infrared and Raman Spectroscopic study of biochemical and chemical treatments of oak wood (*Quercus rubra*) and barley (*Hordeum vulgare*) straw. *J. Agric. Food Chem.* **43**, 2219–2225.

Talbot, N.J. (2003) On the trail of a cereal killer: investigating the biology of *Magnaporthe grisea*. *Annu. Rev. Phytopathol.* **57**, 177–202.

Taylor, J., King, R.D., Altmann, T. and Fiehn, O. (2002) Application of metabolomics to plant genotype discrimination using statistics and machine learning. *Bioinformatics*, **18**(Suppl. 2), S241–S248.

Thines, E., Weber, R.W.S. and Talbot, N.J. (2000) MAP kinase and protein kinase A-dependent mobilization of triacylglycerol and glycogen during appressorium turgor generation by *Magnaporthe grisea*. *Plant Cell*, **12**, 1703–1718.

Umemura, K., Ogawa, N., Shimura, M., Koga, J., Usami, H. and Kono, T. (2003) Possible role of phytocassane, rice phytoalexin, in disease resistance of rice against the blast fungus *Magnaporthe grisea*. *Biosci. Biotechnol. Biochem.* **67**, 899–902.

Urbanczyk-Wochniak, E., Luedemann, A., Kopka, J., Selbig, J., Roessner-Tunali, U., Willmitzer, L. and Fernie, A.R. (2003) Parallel analysis of transcript and metabolic profiles: a new approach in systems biology. *EMBO Rep.* **4**, 989–993.

Vaidyanathan, S., Rowland, J.J., Kell, D.B. and Goodacre, R. (2001) Discrimination of aerobic endospore-forming bacteria via electrospray-ionisation mass spectrometry of whole cell suspensions. *Anal. Chem.* **73**, 4134–4144.

Vaidyanathan, S., Kell, D.B. and Goodacre, R. (2002) Flow-injection electrospray ionization mass spectrometry of crude cell extracts for high-throughput bacterial identification. *J. Am. Soc. Mass Spectrom.* **13**, 118–128.

Weckwerth, W., Loureiro, M.E., Wenzel, K. and Fiehn, O. (2004) Differential metabolic networks unravel the effects of silent plant phenotypes. *Proc. Natl Acad. Sci. USA*, **101**, 7809–7814.

van Wijk, K.J. (2001) Challenges and prospects of plant proteomics. *Plant Physiol.* **126**, 501–508.

Wold, H. (1966) Estimation of principal components and related models by iterative least squares. In *Multivariate Analysis* (Krishnaiah, K.R., ed.). New York: Academic Press, pp. 391–420.

Zhang, W., Wany, C., Qin, C., Wood, T., Olafsdottir, G., Welti, R. and Wang, X. (2003) The oleate-stimulated phospholipase D, PLDδ, and phosphatidic acid decrease H_2O_2-induced cell death in *Arabidopsis*. *Plant Cell*, **15**, 2285–2295.